J. Fluid Mech. (2010), *vol.* 647, *pp.* 125–142.
doi:10.1017/S0022112010000078

Regimes of thermocapillary migration of droplets under partial wetting conditions

J. M. GOMBA† AND G. M. HOMSY

Department of Mechanical Engineering, University of California, Santa Barbara, California 93106-5070, USA

(Received 24 June 2009; revised 18 December 2009; accepted 28 December 2009)

We study the thermocapillary migration of two-dimensional droplets of partially wetting liquids on a non-uniform heated substrate. An equation for the thickness profile of the droplet is derived by employing lubrication approximations. The model includes the effect of a non-zero contact angle introduced through a disjoining–conjoining pressure term. Instead of assuming a fixed shape for the droplet, as in previous works, here we allow the droplet to change its profile with time. We identify and describe three different regimes of behaviour. For small contact angles, the droplet spreads into a long film profile with a capillary ridge near the leading edge, a behaviour that resembles the experiments on Marangoni films reported by Ludviksson & Lightfoot (*Am. Inst. Chem. Eng. J.*, vol. 17, 1971, pp. 1166). For large contact angles, the droplet moves as a single entity, weakly distorted from its static shape. This regime is the usual one reported in experiments on thermocapillary migration of droplets. We also show some intriguing morphologies that appear in the transition between these two regimes. The occurrence of these three regimes and their dependence on various parameters is analysed.

1. Introduction

The spreading of liquids on rigid surfaces and inside channels is of interest in a variety of applications such as coating processes and microfluidic devices (Oron, Davis & Bankoff 1997; Stone, Stroock & Ajdari 2004; Darhuber & Troian 2005). Coating processes are usually performed by the application of a body force, such as gravity or centrifugal force, or by using external thermal gradients (Huppert 1982; Cazabat *et al.* 1990; Ehrhard & Davis 1991; Sur, Witelski & Behringer 2004; Gomba *et al.* 2005). In microfluidic devices, the actuation of very small droplets can be accomplished in many different ways such as pneumatic pumping, centrifugation, thermocapillarity and electrowetting, and these have been used successfully to drive flows both in closed channels and on open surfaces (Ho & Tai 1998; Gallardo *et al.* 1999; Sammarco & Burns 1999; Pollack, Fair & Shenderov 2000; Darhuber *et al.* 2003; Sur, Bertozzi & Behringer 2003; Valentino *et al.* 2003). These forces also play a key role in the control of bubbles and droplets in a large number of experiments aboard spacecraft, where the effect of gravity is negligible (Subramanian & Balasubramanian 2001).

† Present address: Instituto de Física Arroyo Seco, UNCPBA and CONICET, 7000 Tandil, Argentina. Email address for correspondence: jgomba@engineering.ucsb.edu

Here we will focus on the thermocapillary actuation of liquids on horizontal surfaces. A temperature gradient in the substrate produces, in turn, a temperature gradient at the liquid–air surface, inducing a surface tension gradient that exerts a hydrodynamic force that moves the droplet from warmer to colder regions. Following the pioneering work of Bouasse (1924), who made drops climb a tilted wire by heating its lower end, many authors have studied the thermocapillary migration of droplets. The experimental studies of Brzoska, Brochard-Wyart & Rondelez (1993) and Chen *et al.* (2005) are relevant here. Both sets of experiments study the motion of droplets on horizontal silicon surfaces. The set-up employed assures a constant temperature gradient at the substrate and a constant stress at the liquid–air interface. Interestingly, in these experiments the droplets move with a constant velocity and a fixed shape. Brzoska *et al.* (1993) employ polydimethylsiloxane (PDMS) on a hydrophobic surface, with measured contact angles $11^\circ \leqslant \theta \leqslant 13^\circ$. The dependence of the contact angle with temperature T is experimentally found to be negligible, typically $(1/\theta)(\mathrm{d}\theta/\mathrm{d}T) \approx 10^{-2}K^{-1}$. They conclude that contact angle hysteresis is responsible for the droplet pinning when the thermal gradient imposed on the substrate is below a threshold, as predicted by Ford & Nadim (1994). Above this critical value, the velocity of the droplet is proportional to the temperature gradient and inversely proportional to the viscosity. This suggests that the capillary number, considered as a dimensionless speed, is constant, as is appropriate to Stokes flow. Chen *et al.* (2005) employ organic liquids and also check that, for a given volume of fluid, there is a critical temperature gradient below which the droplet does not move. They compare the experimental results with the predictions from a theoretical expression derived following Ford & Nadim (1994) and find that the fitting of the experimental values is more sensitive to contact angle hysteresis than to the magnitude of the slip length.

Recently, Pratap, Moumen & Subramanian (2008) reported experiments of decane droplets on a PDMS-coated surface. In contrast with previous experimental works, here the contact angle is very sensitive to the temperature, changing from 3° to 8° when the temperature is changed from 15° to 50°C. Furthermore, evaporation is not negligible in their experiments, resulting in a loss of mass that reduces the velocity of the droplet with time. These two effects, the dependence of the contact angle with temperature and evaporation, are not considered in our work and so our results will not be applicable to these experiments.

Marangoni wetting films climbing a plate against gravity by thermally induced surface-tension gradients constitute another example of thermocapillary actuation of fluid (Ludviksson & Lightfoot 1971; Teletzke, Davis & Scriven 1987; Kataoka & Troian 1998; Schwartz 2001). The main difference between this and the 'constant-volume' droplet problem is that in Marangoni films there is a continuous pumping of fluid from a container towards the advancing front. The typical liquid profile is characterized by a long film connecting the bulk of fluid with a capillary ridge formed at the leading edge. Ludviksson & Lightfoot (1971) studied the evolution of these films and found that the substrate is coated at a constant rate. The discrepancies between the calculated velocity and experimental values, by up to 40 % in one case, were analysed by Teletzke *et al.* (1987) and Kataoka & Troian (1998), who developed a lubrication model to predict both the velocity and shape of the film. Schwartz (2001) extended these studies by including the effect of partial wetting in order to predict the critical contact angle that stops the flow. As we shall see, these Marangoni film-type profiles will be relevant to the drop migration problem in certain parameter ranges.

These experiments can lead one to conclude falsely that the only difference between the dynamics of droplet and Marangoni films flows is that the former conserves the

mass while the latter does not. However, the fact that the experiments in Marangoni film flows are performed using wetting fluids while the actuation of droplets is typically carried out for partially wetting liquids suggests that wettability may play an important role. In order to examine this point, we present results on the study of the effect of non-zero contact angle θ (partial wettability) on the thermocapillary actuation of droplets. In particular, we discover important differences in flows with low and high contact angle.

Many authors have studied thermocapillary flows involving droplets on solids theoretically. The problem is usually simplified to the study of a two-dimensional droplet under the influence of a shear stress at the liquid–air interface, the flow being solved within the lubrication theory. Steve Davis and his collaborators have done much to develop this approach and to use it to understand fundamental aspects of liquids spreading on isothermal and non-isothermal substrates. Ehrhard & Davis (1991) studied the spreading of liquids driven by a mismatch between the initial and equilibrium contact angles. Using lubrication theory, they were able to account for a variety of physical effects, including thermocapillarity which is of interest in this paper. They considered the spreading of a droplet when the temperature of the substrate, T_w, is higher, the same or lower than the temperature of the surrounding air, T_∞. Assuming a finite thermal resistance at the air–liquid interface, they found that for $T_w > T_\infty$ the Marangoni stress slows the spreading when compared with the case $T_w = T_\infty$, and vice versa for $T_w < T_\infty$. Since there is no overall temperature gradient, the Marangoni stresses do not migrate the droplet, which is our interest here. A later study by Anderson & Davis (1995) extended these concepts to the case of symmetric spreading due to a combination of thermocapillarity and evaporation.

Models of thermocapillary migration of droplets have been developed by Brochard (1989), Ford & Nadim (1994) and Smith (1995). Brochard (1989) analyses the motion of droplets on solid surfaces when the displacement of the fluid is achieved by either chemical or thermal gradients. She assumes a negligible deformation of the shape of the droplet, which is further approximated as a wedge. These hypotheses allow her to compute the force exerted on the droplet and, from that, the velocity of displacement. In order to avoid the divergent stress at the contact line, the integration of the force is done up to a point close, but not all the way, to the contact line. Ford & Nadim (1994) generalize the work of Brochard (1989) to droplets with any arbitrary (fixed) shape and allow different contact angles at the leading and rear fronts. The divergence of the stress is avoided by allowing slip at the contact line. The velocity is assumed to be constant and the derived analytical expression predicts that the difference between the rear and leading contact angle is responsible for the existence of a threshold depinning force. Smith (1995) also treats the thermocapillary migration of a two-dimensional droplet assuming a Navier slip condition but, in addition, he applies a dynamic boundary condition that relates the actual contact angle with the contact line speed (Dussan 1979). Considering flows in the limit of zero capillary numbers, he identifies two steady-state solutions: one corresponding to a pinned droplet with a circulation flow and the other consisting of a droplet translating with constant velocity and shape.

Our objectives are to understand the effect of contact angle and Marangoni number on the regimes of behaviour for migration of drops, and to establish the connection, if any, between Marangoni films and drop migration.

The article is organized as follows. In § 2 we explain the assumptions used in the modelling and derive a general evolution equation for the thickness h. Some details of the numerical procedure employed to solve the equation are given in a subsection.

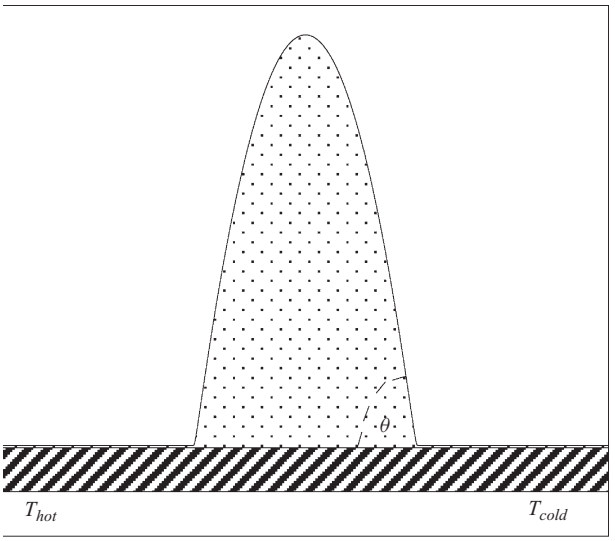

FIGURE 1. Scheme of a two-dimensional droplet on a substrate. The temperature on the substrate linearly decreases from left to right.

An improvement on previous theoretical analyses is that here, instead of considering a droplet moving with a constant velocity and a steady shape as usually assumed, we solve an initial value problem for the thickness h and motion of the droplet, imposing restrictions neither on the velocity of both the contact lines and the drop nor on the drop shape. In § 3 we describe the regime for small contact angles, characterized by a continuous elongation reminiscent of Marangoni films. A self-similar solution for the shape of the droplet is presented and compared with the profile obtained by solving the full equation for h. In § 4 we find a second regime for large contact angles in which the droplet keeps a steady shape. In this regime, the droplet velocity is constant and the dependence with the various parameters of the flow is explored. The behaviour of the droplet for intermediate values of contact angle is presented in § 5. Section 6 concerns the dependence of the regime maps on the droplet size and the temperature gradient.

2. Formulation

We use standard lubrication theory which reduces the Navier–Stokes equations to a single evolution equation for the thickness $h(x, t)$. Although strictly valid for small slope (vanishing contact angles), lubrication theory has proved to be qualitatively, and in some cases, quantitatively correct well outside its formal region of validity. Comparisons between full Stokes flow simulations and lubrication theory, together with discussions of its use for partial wetting conditions, can be found in Mitlin & Petviashvili (1994); Schwartz (1998); Schwartz & Eley (1998); Perazzo & Gratton (2004); Chen *et al.* (2005); Gotkis *et al.* (2006); Diez & Kondic (2007). Thus, in spite of the approximations of lubrication theory, it remains the convenient method of choice for an exploration of the qualitative nature of solutions.

Consider a two-dimensional droplet deposited on a horizontal substrate which is subject to a constant temperature gradient, as shown in figure 1. The velocity $u(x, z, t)$

in the x direction is related to the pressure p by

$$\frac{\partial p}{\partial x} = \mu \frac{\partial^2 u}{\partial z^2}, \tag{2.1}$$

where μ is the viscosity of the liquid and p is given by

$$p = -\gamma \frac{\mathrm{d}^2 h}{\mathrm{d}x^2} - \Pi. \tag{2.2}$$

Here, γ is the surface tension and Π is the disjoining–conjoining pressure defined by

$$\Pi = \kappa \left[\left(\frac{h_*}{h} \right)^n - \left(\frac{h_*}{h} \right)^m \right], \tag{2.3}$$

where

$$\kappa = \frac{S(m-1)(n-1)}{(n-m)h_*}, \tag{2.4}$$

h_* is the thickness of the energetically favoured molecular film (Churaev & Sobolev 1995; Glasner & Witelski 2003; Gomba & Homsy 2009) and S is the spreading parameter. The use of a disjoining–conjoining model for the molecular interactions between fluid and substrate has been discussed by Mitlin & Petviashvili (1994) and Schwartz & Eley (1998). Its use here has several advantages over previous studies of drop migration, the most important of which are as follows: (i) elimination of the need to model the dynamic contact angle and the singularity with the no-slip condition due to the presence of a precursor film (as a result of the favourable interaction) and (ii) the ability of the model to prescribe an apparent contact angle as an independent parameter. The spreading parameter S can be related to the contact angle θ via the Laplace–Young condition as $S = \gamma(1 - \cos\theta)$ (Schwartz & Eley 1998).

In the usual fashion, the surface tension γ is taken to be linear in the temperature T at the air–liquid interface

$$\gamma = \gamma_0 - \sigma(T - T_0), \tag{2.5}$$

with γ_0 being the surface tension at $T = T_0$ and σ being a positive constant.

The velocity $u(x, z, t)$ is subject to the boundary conditions of no slip and the tangential stress condition, respectively:

$$u(x, 0, t) = 0, \tag{2.6}$$

$$\mu \left. \frac{\partial u}{\partial z} \right|_{z=h} = \frac{\mathrm{d}\gamma}{\mathrm{d}x} \equiv \left. \frac{\mathrm{d}\gamma}{\mathrm{d}T} \frac{\mathrm{d}T}{\mathrm{d}x} \right|_{z=h}. \tag{2.7}$$

In order to relate the unknown temperature T at the interface to the known temperature profile at the substrate, T_s, we adopt two common assumptions (Brochard 1989; Ford & Nadim 1994). The first is that conduction is the main heat transfer mechanism within the drop, i.e. the Péclet number, $Pe = h_c U/\alpha$, is small. Under this assumption the temperature profile inside the droplet is linear in z (Ehrhard & Davis 1991) and the temperature at the surface is given by

$$T(x, h) = \frac{T_s(x)}{1 + Bi\, h}. \tag{2.8}$$

Here, $Bi = q_s h_c / k_l$ is the Biot number, where q_s is the surface heat transfer coefficient at the air–liquid interface and k_l is the conductivity coefficient of the liquid. The second assumption is that $Bi\, h \ll 1$, which is realistic for most experiments (Cazabat *et al.*

1990; Brzoska *et al.* 1993; Sur *et al.* 2003, 2004; Chen *et al.* 2005): for example, values of Bi are estimated by Chen *et al.* (2005) to be between 0.02 and 0.06 for their experiments. Thus, $T(x,h)=T_s(x)$. Consistent with the experiments of Brzoska *et al.* (1993) and Chen *et al.* (2005), we prescribe a linear dependence of T_s with x, and so the boundary condition (2.7) becomes

$$\mu\frac{\partial u}{\partial z}\bigg|_{z=h}=\tau, \tag{2.9}$$

where $\tau=(\mathrm{d}\gamma/\mathrm{d}T_s)(\mathrm{d}T_s/\mathrm{d}x)$ is a constant.

Determining the velocity u by integrating (2.1) subject to the boundary conditions (2.6) and (2.7) and applying conservation of mass results in the following standard equation for the thickness h:

$$\frac{\partial h}{\partial t}+\frac{\gamma}{3\mu}\frac{\partial}{\partial x}\left(h^3\frac{\partial^3 h}{\partial x^3}\right)\frac{\kappa}{3\mu}\frac{\partial}{\partial x}\left(h^3\frac{\partial}{\partial x}\left[\left(\frac{h_*}{h}\right)^n-\left(\frac{h_*}{h}\right)^m\right]\right)+\frac{\tau}{2\mu}\frac{\partial h^2}{\partial x}=0. \tag{2.10}$$

This is the generic thin film equation for flow driven by a constant shear stress τ (Eres, Schwartz & Roy 2000). Defining the dimensionless variables $\hat{x}=x/x_c$, $\hat{h}=h/h_c$ and $\hat{t}=t/t_c$ with $t_c=3\mu x_c^4/(\gamma h_c^3)$ and taking $(n,m)=(3,2)$ (Glasner & Witelski 2003; Diez & Kondic 2007), (2.10) becomes

$$\frac{\partial h}{\partial t}+\frac{\partial}{\partial x}\left(h^3\frac{\partial^3 h}{\partial x^3}\right)+K\frac{\partial}{\partial x}\left(h^3\frac{\partial}{\partial x}\left[\left(\frac{h_*}{h}\right)^3-\left(\frac{h_*}{h}\right)^2\right]\right)+B\frac{\partial h^2}{\partial x}=0, \tag{2.11}$$

where we have dropped the hats for simplicity. The parameters K and B are defined as

$$\left.\begin{aligned}K&=\frac{2(1-\cos\theta)}{h_*}\frac{x_c^2}{h_c^2},\\ B&=\frac{3\tau}{2\gamma_0}\frac{x_c^3}{h_c^2},\end{aligned}\right\} \tag{2.12}$$

with h_* in units of h_c. At this point we have some freedom to choose the length scales h_c and x_c. While there appears to be three parameters, K, B and h_*, by using the intrinsic scales employed by Schwartz, Roux & Cooper-White (2005) (in a slightly different context), or those of Gomba & Homsy (2009), it is possible to reduce the number of dimensionless parameters to two. But for ease of comparison with experimental data, we define $h_c=x_c=a$, where $a=\sqrt{\gamma_0/\rho g}$ is the capillary length. We mention the simplifications associated with using intrinsic scales below when appropriate.

2.1. *Computational issues*

We discretize (2.11) in space using regular centred finite differences except for the fourth-order term, for which central differencing does not necessarily preserve the positivity of the solution, i.e. h can evolve from positive to negative values (Bernis, Peletier & Williams 1992; Beretta, Berstch & Passo 1995). Accordingly, we implement a 'positivity preserving scheme' proposed by Zhornitskaya & Bertozzi (2000). The resulting system of equations are evolved in time by employing a synchronized marching Crank–Nicholson scheme combined with an adaptive time stepping procedure (Gomba *et al.* 2007). The corresponding pentadiagonal matrix is solved by using routines extracted from Press *et al.* (1992; the routines used in this

work are 'bandec' and 'banbks'), and the boundary conditions at both extremes of the domain, $x = 0$ and $x = L$, are

$$\left.\frac{\mathrm{d}h}{\mathrm{d}x}\right|_{x=0,L} = \left.\frac{\mathrm{d}h^3}{\mathrm{d}x^3}\right|_{x=0,L} = 0. \tag{2.13}$$

We note that any attempt to quantitatively reproduce experimental conditions requires the choice of an appropriate value for the dimensional molecular film thickness, $h_* h_c$, which typically is of the order of 10 nm. On the other hand, it is well known that the space step Δx must be of the same order of h_* (Schwartz & Eley 1998; Diez & Kondic 2001). If the length of the domain is about 10 cm, the mesh would consist of 10^8 collocation points. This large number results in long time-consuming calculations even when carried out on fast workstations. As an example of the computing times, a case with dimensionless cross-sectional area $A = 10$, $h_* = 0.005$, $\theta = 30^\circ$ and $\Delta x = 0.01$ in a domain of dimensionless length $L = 100$ required 4 days to be solved on an Intel Xeon CPU 3.60 GHz processor. The time increases even more for lower values of h_* or larger values of θ. With the aim of spending reasonable computing times, most cases were solved with $h_* \geqslant 5 \times 10^{-3}$, and $\Delta x = 0.01$. Even though this range of h_* is not a realistic value, we will show that it allows us to reproduce the features reported in experiments. We also did a modest parameter study to find that the dependence of the results on h_* is much weaker than that of other parameters.

In order to establish relevant values of the parameter B, we recall the experimental conditions reported by Brzoska *et al.* (1993) and Chen *et al.* (2005). In those experiments, the ranges of values for the quantities involved in the definition of B are: $20 \times 10^{-3}\,\mathrm{N m^{-1}} \leqslant \gamma \leqslant 30 \times 10^{-3}\,\mathrm{N m^{-1}}$, $0.05 \times 10^{-3}\,Nm^{-1}{}^\circ C \leqslant \mathrm{d}\gamma/\mathrm{d}T \leqslant 0.1 \times 10^{-3}\,Nm^{-1}{}^\circ C$ and $3.5^\circ\mathrm{C\,cm^{-1}} \leqslant \mathrm{d}T_s/\mathrm{d}x \leqslant 36^\circ\mathrm{C\,cm^{-1}}$. Thus, the parameter B can be considered to be in the interval $(0.002 - 0.03)$.

We also estimate the cross-sectional area of the 'three-dimensional' droplets in the experiments of Brzoska *et al.* (1993) and Chen *et al.* (2005) by considering the section at the symmetry plane that crosses the point of maximum thickness. This gives us an idea of the cross-sectional area to use in our 'two-dimensional' problem. For a three-dimensional droplet with a radius R, measured at the liquid–substrate interface, this area is given by

$$A = R^2\,(\theta/\sin\theta - \cos\theta)\,/\,\sin\theta. \tag{2.14}$$

Accordingly, the dimensionless cross-sectional area in the experiments of Brzoska *et al.* (1993) can be estimated to be within the range $0.18 \leqslant A \leqslant 6.3$. The experiments of Chen *et al.* (2005) also fall within that range, typically $0.34 \leqslant A \leqslant 0.4$.

In the next three sections, we describe the different regimes we observe by first fixing all dimensionless parameters but θ at the following values: $A = 10$, $B = 0.01$ and $h_* = 0.01$. The initial condition always corresponds to the shape of a static droplet of area A when the temperature gradient is zero (Gomba & Homsy 2009), and we then follow the evolution after a step increase in the value of B.

3. Film regime: small contact angle

Figure 2 presents the numerical solution of (2.11) for a small contact angle, $\theta = 5^\circ$, which shows that the leading front moves faster than the rear one, thus the width increases with time. Interestingly, after a transient stage, the bulk region exhibits a linear profile with a slope that decreases in time, and the leading edge shows a

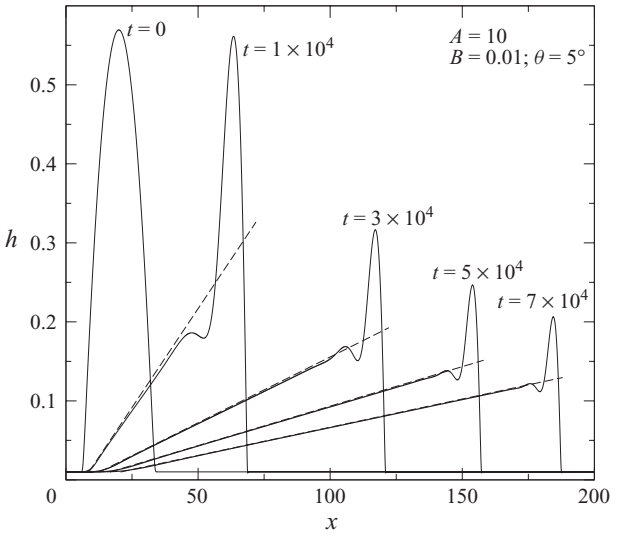

FIGURE 2. Evolution of the thickness profile obtained by solving (2.11) (solid lines) and the asymptotic profiles given by (3.5) (dashed lines). The profiles correspond to the case with $\theta = 5°$, $A = 10$, $B = 0.01$ and $h_* = 0.01$.

characteristic capillary ridge. Such behaviour is similar to what is seen in Marangoni films:hence we refer to this as the film regime.

The behaviour away from the leading and trailing edges can be captured by a simple self-similar solution. On the one hand, the small value of θ suggests that the disjoining–conjoining pressure is negligible. On the other hand, the numerical solution shows that the curvature in the bulk region is small and therefore the capillary pressure term is also negligible. Dropping both terms, (2.11) becomes

$$\frac{\partial h}{\partial t} + B\frac{\partial (h^2)}{\partial x} = 0. \tag{3.1}$$

We seek a self-similar solution of the following form (Barenblatt 1996)

$$h = t^p H(\zeta), \tag{3.2}$$

$$x = \zeta\, x_N, \tag{3.3}$$

where $x_N = t^q$ is the position of the leading front and p, q are constants. Requiring that time enters only in the form given in (3.2) and (3.3) and that the volume remains constant, the power law exponents are found to be $q = -p = 1/2$. As a consequence, (3.1) becomes

$$-\left(H + \zeta\frac{\mathrm{d}H}{\mathrm{d}\zeta}\right) + 2B\frac{\mathrm{d}H^2}{\mathrm{d}\zeta} = 0. \tag{3.4}$$

Integrating, applying the condition $H(0) = 0$, and recovering the original variables, we find:

$$h = \frac{x}{2Bt} \quad \text{for} \quad x_R \leqslant x \leqslant x_A. \tag{3.5}$$

Here the positions for the rear and advancing fronts, x_R and x_A, are given by

$$\left.\begin{aligned} x_R &= x_0 + 2h_{film}Bt, \\ x_A &= x_R + \sqrt{4ABt}. \end{aligned}\right\} \tag{3.6}$$

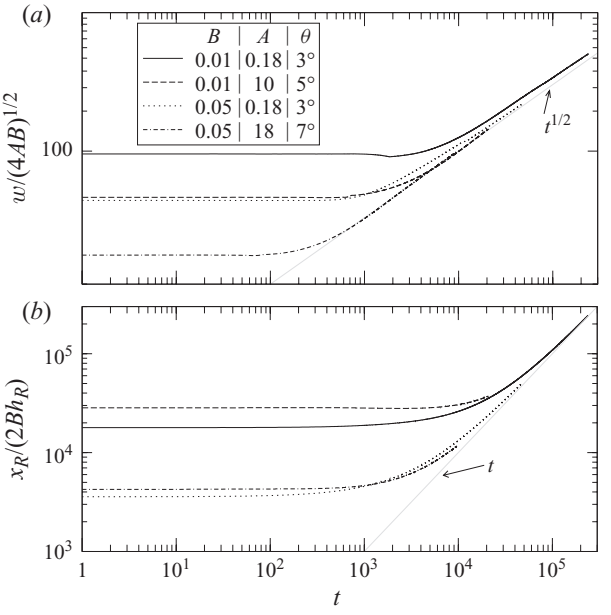

FIGURE 3. Evolution of (*a*) w and (*b*) x_R for different combinations of B, A and θ. The grey lines represent the asymptotic power law predicted by (3.8) and (3.6), respectively.

Considering that the area A of the droplet is given by the area of the triangle defined in (3.5) and introducing the notation $h_A = x_A/2Bt$ and $h_R = x_R/2Bt$, it is possible to write

$$A = \frac{w(h_A - h_R)}{2} = \frac{w^2}{4Bt}, \tag{3.7}$$

from where the width $w = x_A - x_R$ of the droplet is given by

$$w = (4ABt)^{1/2}. \tag{3.8}$$

Figure 2 shows the comparison of the complete profile with the asymptotic profile defined by (3.5) and (3.6). There is a reasonably good prediction of the slope of the profile in the bulk region away from the capillary ridge. Despite the fact that the experimental literature does not report cases with this particular contact angle, experiments carried out by Sur *et al.* (2003) for Marangoni films of wetting liquids have shown, at least in one case, a linear profile connecting the advancing ridge with the fluid in the container (see figure 5 in Sur *et al.* 2003).

In figure 3(*a*,*b*) we show the evolution of w and x_R for different values of A and θ. Notice that, in general, w reaches the asymptotic law given in (3.6) faster than x_R. The delay in x_R in approaching the asymptotic behaviour is due to the fact that close to the contact line neither the curvature nor the disjoining pressure is completely negligible.

Summarizing, it is found that for small contact angles, the droplet increases its width with time and a linear profile is developed as a result of the competition between Marangoni and viscous stresses. Only the rear contact line advances asymptotically with a constant velocity.

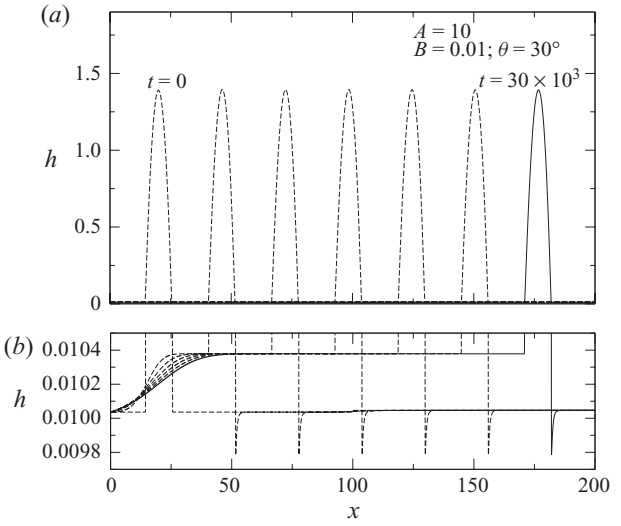

FIGURE 4. Evolution of the droplet profile with $\theta = 30°$, $A = 10$, $B = 0.01$ and $h_* = 0.01$. (a): Quasi-steady droplet motion with constant velocity shown at equal time intervals. The solid line represents the last profile for $t = 30 \times 10^3$. (b): A zoom of the region close to the substrate.

4. Droplet regime: large contact angle

Figure 4(a) shows the displacementof a droplet with $\theta = 30°$. Contrary to what we observed for small contact angles, the droplet moves as a whole to a good approximation keeping its original steady shape. Hence we refer to this as the droplet regime. Here the effect of the disjoining–conjoining pressure is stronger than in the previous case and the Marangoni stress induced at the liquid–air interface cannot change the shape of the droplet. Interestingly, when we observe the region close to the substrate in detail, we detect that the droplet leaves a constant-thickness thin film behind the rear front. An example is shown in figure 4(b), which is a zoom of the region close to the substrate. In this case, the film behind the advancing droplet attains a thickness of ≈ 0.01038. The height of this film decreases when either θ or A is increased.

One of the main features in this regime is that both front and rear move with the same 'constant' velocity. The natural question is how this velocity depends on the parameters A, B, θ and h_*. On the face of it, five-'dimensional' parameters determine the flow in the droplet regime: μ, τ, $h_{*,dim}$, A_{dim} and U_{dim}. However, as mentioned above, the use of intrinsic scales reduces the number of dimensionless parameters by two. Thus guided by the form of the constant κ, the natural scales of the steady problem (Gomba & Homsy 2009), and dimensional analysis, two Π groups can be constructed that lead to the following relationship,

$$\frac{U_{dim}\mu}{\tau h_{*,dim}} = f\left(\frac{A_{dim}\sqrt{2(1-\cos\theta)}}{h_{*,dim}^2}\right). \tag{4.1}$$

This expression can be easily rewritten in terms of the 'dimensionless' parameters A, B, θ and h_*, leading to the following equation:

$$\frac{U}{Bh_*} = f'\left(\frac{A\sqrt{2(1-\cos\theta)}}{h_*^2}\right). \tag{4.2}$$

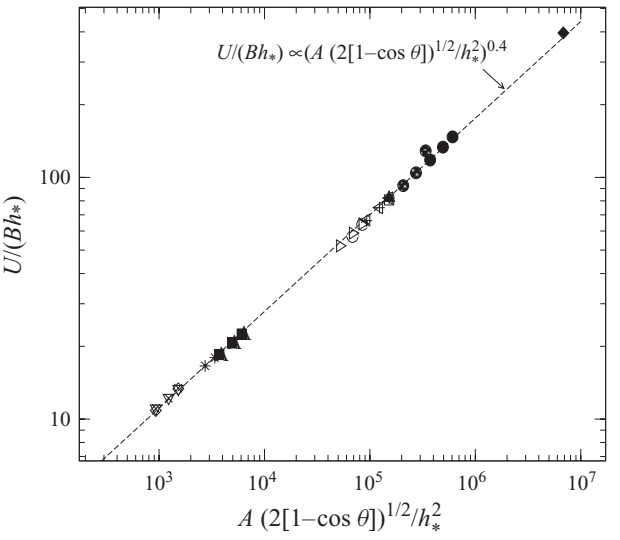

FIGURE 5. Dependence of U on the problem parameters A, B, θ and h_*. The points represent 39 different combinations of the parameters, whose values are $A = 0.18; 10; 18$, $B = 0.002; 0.01; 0.05$; $\theta = 30^\circ; 40^\circ; 50^\circ$ and $h_* = 0.001; 0.005; 0.01; 0.05$.

Figure 5 shows the dependence of U on the dimensionless parameter $A\sqrt{2(1-\cos\theta)}/h_*^2$ for several different combinations of the parameters involved. The plot shows that there is a power law dependence between these quantities given by

$$U \propto Bh_* \left(\frac{A\sqrt{2(1-\cos\theta)}}{h_*^2} \right)^{0.4}. \tag{4.3}$$

We currently do not have any theoretical explanation for the power law exponent, but further research into travelling wave solutions for small B may be instructive on this point.

Figure 6(a,b) shows the dependence on B of the contact angles at the rear and the advancing fronts, θ_R and θ_A, for two different areas (the contact angles are normalized to the value they would have for $B = 0$). For $B = 0.002$, both θ_R and θ_A show a slight increase from the value corresponding to $B = 0$. For larger values of B, θ_A increases while θ_R decreases. Notice that for $A = 10$ (figure 6a), the percentage change of the contact angle with B is higher than for $A = 0.18$ (figure 6b).

Concluding this section, for large contact angles the droplet moves at constant speed while to a good approximation keeping its initial shape, indicating the dominance of the disjoining–conjoining pressure of the distortion due to the Marangoni flow. At the same time, a thin constant-thickness film is left behind the droplet. The droplet moves with a constant velocity which is proportional to B and inversely proportional to the viscosity, in agreement with experimental results of Brzoska *et al.* (1993) and Chen *et al.* (2005).

5. The transition regime

This regime pertains to intermediate values of θ. In the previous two sections we show that the thickness profile for small values of θ is determined by Marangoni stresses while, in the opposite limit of large θ, the disjoining–conjoining pressure

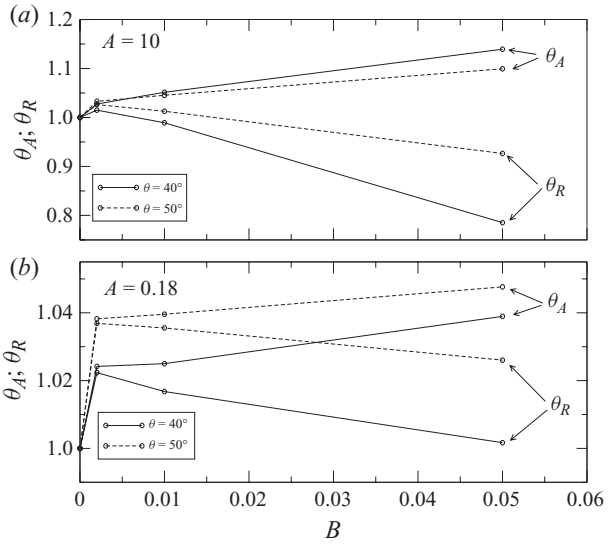

FIGURE 6. Contact angles at the rear and advancing fronts, θ_R and θ_A, respectively, normalized to the value of the contact angle for $B = 0$, for two different areas: (*a*) $A = 10$ and (*b*) $A = 0.18$.

term is responsible for maintaining the initial droplet shape. Intermediate values of θ correspond to a regime where both Marangoni term and disjoining–conjoining pressure compete and, accordingly, the behaviour is transient and complex. Figure 7 shows the evolution of the profile for $\theta = 10^\circ$. The droplet first develops a linear profile but at a time close to $t = 4 \times 10^4$, small droplets detach from the rear front. At the same time, the region connecting the bulk and the front ridge decreases its thickness, which ultimately produces a break-up at the leading edge. At the end of the computation, we have a large number of very small droplets in the rear region, the bulk of the original droplet and a large droplet at the front. It is clear that, in this regime, the Marangoni and disjoining–conjoining terms compete, the first trying to keep a straight profile and the second inducing a rupture into smaller cylindrical droplets.

Figure 8 shows another behaviour, here observed for $\theta = 16^\circ$, for which the strength κ of the disjoining–conjoining pressure increases. The droplet immediately breaks up into two droplets which then travel with nearly constant shape. The rear droplet adopts a cylindrical shape while the leading one adopts a non-standard shape. After a transient, the rear droplet travels faster than the leading one.

The occurrence of non-cylindrical shapes does not necessarily appear after a break-up process. For example, for $A = 18$ and $\theta = 18^\circ$, the break-up does not occur, as shown in figure 9. At the beginning, the droplet seems to evolve toward a break-up into two droplets, but it ultimately adopts a non-standard shape (with three local maxima) that travels with a constant velocity.

To summarize, we find that the thermocapillary migration for intermediate contact angles is very complex and difficult to characterize in a simple fashion. Most of the cases studied did not yield a steady state or a simple spreading behaviour, but rather exhibited complicated time dependence and a tendency toward film rupture. As we will show below, most of the experiments are not in the range of parameters that results in the intermediate regime. Additionally, there may be differences between break-ups in two and three dimensions. For these reasons, we leave a detailed study

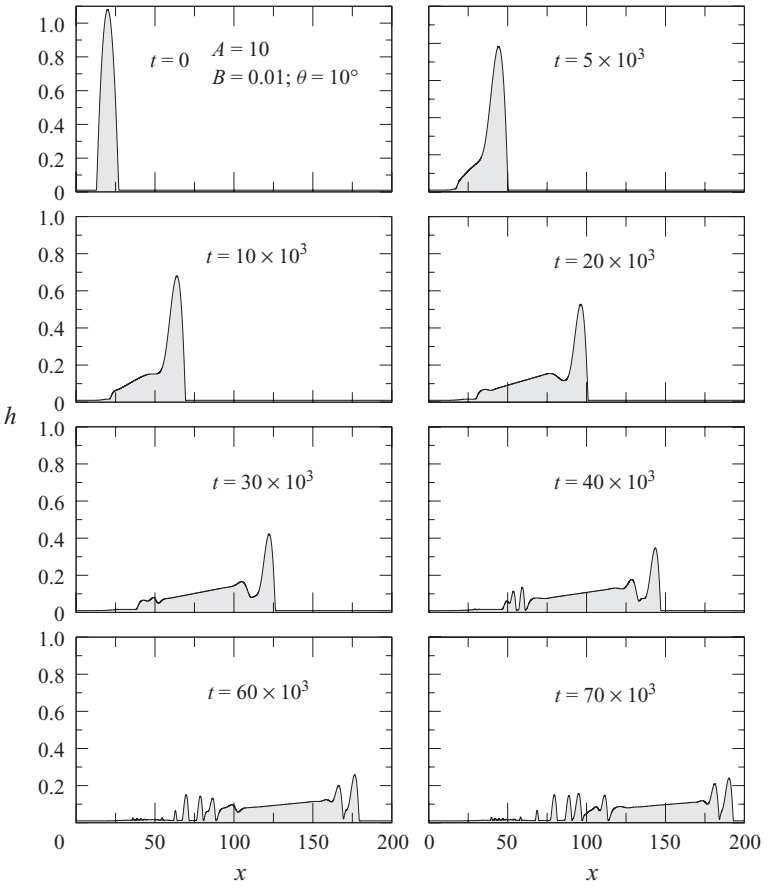

FIGURE 7. Evolution of the droplet profile for $\theta = 10^\circ$ ($A = 10$, $B = 0.01$ and $h_* = 0.01$).

of the break-up for the future when experiments with relatively non-wetting liquids might justify it.

6. Regime maps

Having discovered and characterized the different regimes,we now study how the parameters, A, B and h_*, affect which regime may occur. We do this by representing the different regimes in the θ–A plane, with B as a parameter. Figure 10 shows one of these maps for $B = 0.01$. Notice that all three regimes—film, droplet and transition—can be observed for the range of A studied. Interestingly, due to the fact that the integral effect of the disjoining pressure on the whole volume is more important for smaller droplets than for larger ones, the values of θ at which we observe the transition from film to transition regimes and from transition to droplet regimes are lower for the smaller values of A. For example, for $A = 0.18$, the values of the contact angles which define the boundary between the film–transition and transition–droplet regimes are $\theta_{FT} \approx 5^\circ$ and $\theta_{TD} \approx 7^\circ$, respectively, while the corresponding contact angles for $A = 18$ are $\theta_{FT} \approx 9^\circ$ and $\theta_{TD} \approx 20^\circ$.

These maps help explain why the droplet regime is the only one reported to date. The experiments of Chen *et al.* (2005), for which $B \approx 0.01$, $A \approx 0.37$, are indicated in figure 10. This study observed only the droplet regime, in agreement with our regime

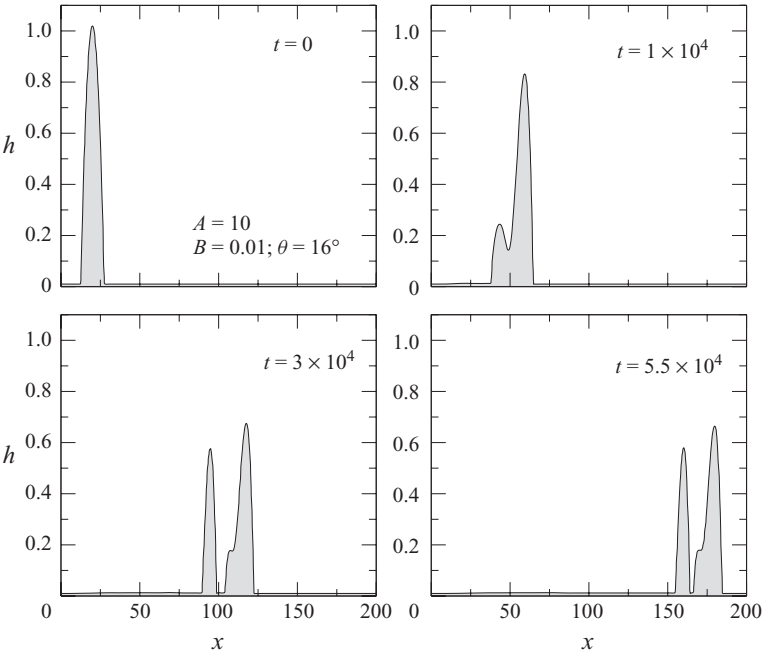

FIGURE 8. Evolution of the droplet profile for $\theta = 16^\circ$ ($A = 10$, $B = 0.01$ and $h_* = 0.01$). The droplet breaks into two smaller droplets.

map. Figure 10 also suggests that the highest values of A in experiments of Brzoska *et al.* (1993) fall in thetransition regime, but those experiments were performed with smaller values of B: the more relevant comparison is with figure 11.

Figure 11(a, b) presents the same diagram but for $B = 0.05$ and $B = 0.002$, respectively. We can observe that when the value of B is decreased (increased), the contact angles θ_{FT} and θ_{TD} reduce (increase) their values. The results for $B = 0.002$ bring the theory and the experiments of Brzoska *et al.* (1993) into agreement: the film regime disappears for small values of A, a result that is consistent with these experiments (for which $0.002 \leqslant B \leqslant 0.007$), all of which fall in the droplet regime.

We also explored the effect of h_*, solving all the same cases presented in figure 10 but using $h_* = 0.005$. Only for the transition regime do we observe differences (basically in the number and shape of the detached droplets), and we do not detect any important change in the values of the contact angles, θ_{FT} and θ_{TD}, respectively, that define the boundaries of the film–transition and transition–droplet regimes. We conclude that in spite of the fact that our numerical values of h_* are larger than appropriate to a film of molecular thickness, the simulations capture the different regime maps in a qualitative way and that they depend more strongly on the other parameters of the problem.

7. Conclusions

In this paper, we have considered the thermocapillary migration of droplets on horizontal surfaces. We employed lubrication theory to derive an equation for the droplet profile that includes the effect of the disjoining–conjoining pressure. The form of the chosen disjoining–conjoining pressure term admits a non-zero contact angle at the contact line region. One of the main differences with previous works is that we do

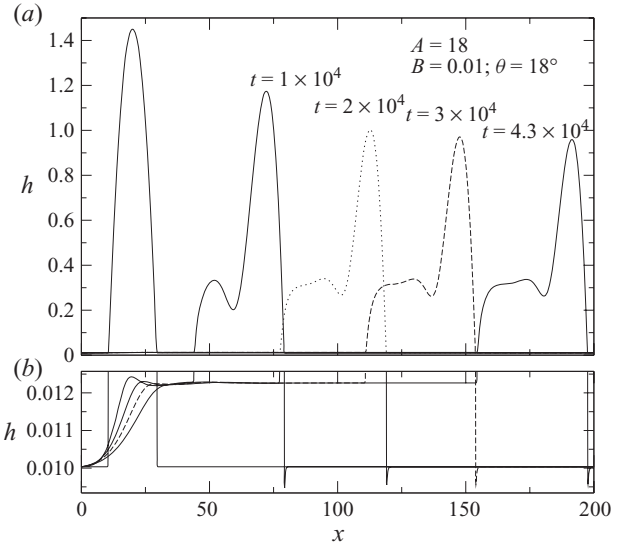

FIGURE 9. (*a*) Evolution of the droplet profile for $\theta = 18^\circ$ and $A = 18$ ($B = 0.01$ and $h_* = 0.01$). After a short transient, the droplet travels with a constant velocity, but with a non-standard shape. (*b*) Zoom of the thickness profile close to the substrate. A thin constant-thickness film of approximate thickness 0.012 is left behind the droplet.

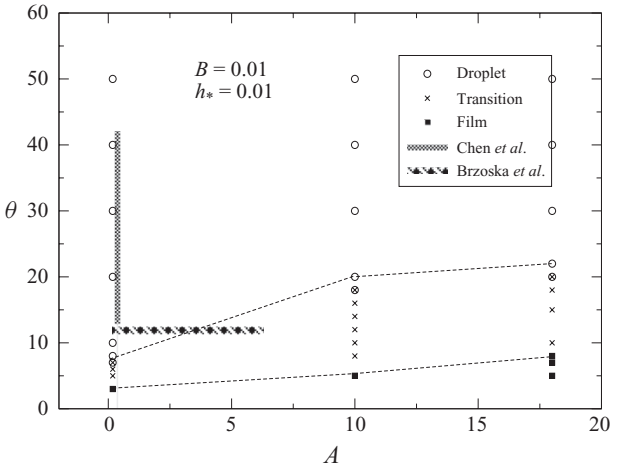

FIGURE 10. Map of the film, droplet and transition regimes in the θ–A space. The experimental data corresponds to the experiments reported in Brzoska *et al.* (1993) and Chen *et al.* (2005). Note that in Brzoska's experiments $0.002 \leqslant B \leqslant 0.007$, i.e. a value of B lower than that of these simulations.

not assume a constant spreading velocity, but rather we allow the droplet to evolve its shape in time.

We find that for small contact angles,the droplet continuously increases its width. The droplet adopts a linear shape in an outer region, a profile that is captured by a self-similar solution. Expressions for the positions of the rear and leading edges are derived via a mass balance. In this regime, Marangoni stresses are responsible for the

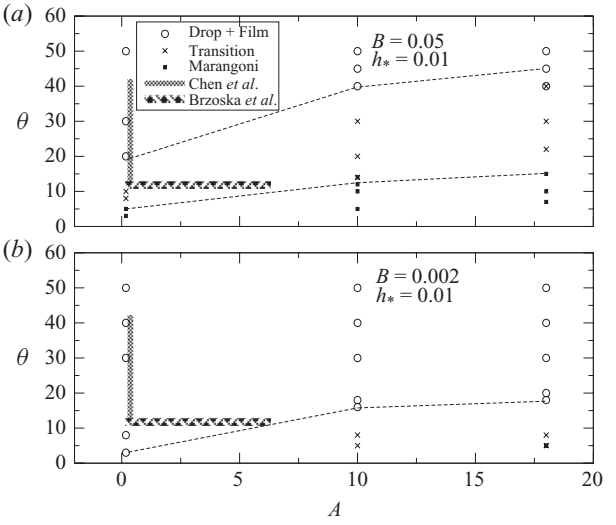

FIGURE 11. Effect of B in the distribution of the flow regimes on the θ–A plane.

linear shape of the thickness profile, the effect of the disjoining–conjoining pressure being negligible.

In contrast, when the contact angle is relatively large, the droplet approximately keeps its steady initial shape and moves at a constant velocity. Combining dimensional analysis and numerical simulations, we find that the velocity follows a power law in dimensionless variables combining the parameters A, B, h_* and θ. The expression for the velocity, given by (4.3), predicts that the droplet speed is proportional to the temperature gradient imposed on the substrate and inversely proportional to the viscosity, in agreement with experimental results of Brzoska *et al.* (1993) and Chen *et al.* (2005). It also predicts that the velocity increases with A, as observed in experiments. Notice that while experiments of Brzoska *et al.* (1993) present a linear dependence with R, the experiments of Chen *et al.* (2005) show a dependence that goes with R^{ℓ}, with $\ell < 1$ indeterminate (see figure 4 in Chen *et al.* 2005). If we consider a cylindrical cap, in our case the velocity is proportional to $R^{0.8}$. We think that the dependence with R varies with the particular fluid employed, so different disjoining–conjoining pressure models may lead to a different dependence with R, θ and h_*. In this regime, the values of the apparent contact angles at the contact leading and rear fronts are found to be dependent on the temperature gradient imposed at the substrate, that is, with the dimensionless parameter B. For small B, we observe that both contact angles increase while for larger B, the rear contact angle decreases while the leading contact angle increases. The relative change is larger for larger droplets. The Marangoni stress moves the droplet from warmer to colder regions, but it does not have any important effect on the shape of the thickness profile: the disjoining–conjoining pressure effect is strong enough to keep the shape of the droplet fixed.

For intermediate values of contact angle, we observe a transition regime in which the dynamics are complicated. Marangoni and disjoining pressure effects compete and a wide number of possible morphologies appear. In this regime, we observe break-up processes, droplets moving with non-standard shapes and also coalescence. A deeper study of this regime is needed in order to answer some open questions, for example,

the conditions under which the break-up occurs and how the volumes of the resulting droplets are selected.

The occurrence of the three regimes is very sensitive to the values of A and B. We display our results in a map in the θ–A plane and find that, for a given B, the limiting contact angle that separates the film-transition and transition-droplet regimes are smaller for smaller A. Employing the same diagram, but for a lower value of B, we observe that these limiting contact angles decrease, and the film regime does not occur even for the smallest contact angle analysed. For large B, the limits move toward higher values of θ. In spite of the relative simplicity of the model, all these trends are in agreement with available experiments.

This work was supported by the US DOE through grant number DE-FG02-05ER15692. JMG gratefully acknowledges the Fulbright Foundation and CONICET for partial support.

REFERENCES

Anderson, D. M. & Davis, S. H. 1995 The spreading of volatile liquid droplets on heated surfaces. *Phys. Fluids* **7** (2), 248–265.

Barenblatt, G. I. 1996 *Scaling, Self-similarity, and Intermediate Asymptotics*. Cambridge University Press.

Beretta, E., Berstch, M. & Passo, R. D. 1995 Nonnegative solutions of a fourth order nonlinear degenerate parabolic equation. *Arch. Ration. Mech. Anal.* **129**, 175.

Bernis, F., Peletier, L. A. & Williams, S. M. 1992 Source type solutions of a fourth order nonlinear degenerate parabolic equation. *Nonlinear Anal. Theory Methods Appl.* **18**, 217.

Bouasse, H. 1924 *Capillarité phénomènes superficiels*. Librairie Delgrave.

Brochard, F. 1989 Motions of droplets on solid surfaces induced by chemical or thermal gradients. *Langmuir* **5** (2), 432–438.

Brzoska, J. B., Brochard-Wyart, F. & Rondelez, F. 1993 Motions of droplets on hydrophobic model surfaces induced by thermal gradients. *Langmuir* **9** (8), 2220–2224.

Cazabat, A. M., Heslot, F., Troian, S. M. & Carles, P. 1990 Fingering instability of thin spreading films driven by temperature gradients. *Nature* **346**, 824.

Chen, J. Z., Troian, S. M., Darhuber, A. A. & Wagner, S. 2005 Effect of contact angle hysteresis on thermocapillary droplet actuation. *J. Appl. Phys.* **97** (1), 014906.

Churaev, N. V. & Sobolev, V. D. 1995 Prediction of contact angles on the basis of the Frumkin–Derjaguin approach. *Adv. Colloid Interface Sci.* **61**, 1–16.

Darhuber, A. A. & Troian, S. M. 2005 Principles of microfluidic actuation by modulation of surface stresses. *Annu. Rev. Fluid Mech.* **37**, 425.

Darhuber, A. A., Valentino, J. P., Davis, J. M., Troian, S. M. & Wagner, S. 2003 Microfluidic actuation by modulation of surface stresses. *Appl. Phys. Lett.* **82** (4), 657–659.

Diez, J. A. & Kondic, L. 2001 Contact line instabilities of thin liquid films. *Phys. Rev. Lett.* **86**, 632.

Diez, J. A. & Kondic, L. 2007 On the breakup of fluid films of finite and infinite extent. *Phys. Fluids* **19** (7), 072107.

Dussan, V. E. B. 1979 On the spreading of liquids on solid surfaces: static and dynamic contact lines. *Annu. Rev. Fluid Mech.* **11**, 317.

Ehrhard, P. & Davis, S. H. 1991 Non-isothermal spreading of liquid drops on horizontal plates. *J. Fluid Mech.* **229**, 365.

Eres, M. H., Schwartz, L. W. & Roy, R. V. 2000 Fingering phenomena for driven coating films. *Phys. Fluids* **12**, 1278.

Ford, M. L. & Nadim, A. 1994 Thermocapillary migration of an attached drop on a solid surface. *Phys. Fluids* **6**, 3183.

Gallardo, B. S., Gupta, V. K., Eagerton, F. D., Jong, L. I., Craig, V. S., Shah, R. R. & Abbott, N. L. 1999 Electrochemical principles for active control of liquids on submillimeter scales. *Science* **283** (5398), 57–60.

Glasner, K. B. & Witelski, T. P. 2003 Coarsening dynamics of dewetting films. *Phys. Rev.* E **67**, 016302.

Gomba, J., Diez, J., González, A. G. & Gratton, R. 2005 Spreading of a micrometric fluid strip down a plane under controlled initial conditions. *Phys. Rev.* E **71**, 016304.

Gomba, J. M., Diez, J., Gratton, R., González, A. G. & Kondic, L. 2007 Stability study of a constant-volume thin film flow. *Phys. Rev.* E **76** (4), 046308.

Gomba, J. M. & Homsy, G. M. 2009 Analytical solutions for partially wetting two-dimensional droplets. *Langmuir* **25** (10), 5684–5691.

Gotkis, Y., Ivanov, I., Murisic, N. & Kondic, L. 2006 Dynamic structure formation at the fronts of volatile liquid drops. *Phys. Rev. Lett.* **97** (18), 186101.

Ho, C.-M. & Tai, Y.-C. 1998 Micro-electro-mechanical systems (MEMS) and fluid flows. *Annu. Rev. Fluid Mech.* **30**, 579.

Huppert, H. 1982 Flow and instability of a viscous current down a slope. *Nature* **300**, 427.

Kataoka, D. E. & Troian, S. M. 1998 Stabilizing the advancing front of thermally driven climbing films. *J. Colloid Interface Sci.* **203**, 335.

Ludviksson, V. & Lightfoot, E. N. 1971 The dynamics of thin liquid films in the presence of surface-tension gradients. *Am. Inst. Chem. Eng. J.* **17**, 1166.

Mitlin, V. S. & Petviashvili, N. V. 1994 Nonlinear dynamics of dewetting: kinetically stable structures. *Phys. Lett.* A **192**, 323–326.

Oron, A., Davis, S. H. & Bankoff, S. G. 1997 Long-scale evolution of thin liquid films. *Rev. Mod. Phys.* **69**, 931.

Perazzo, C. A. & Gratton, J. 2004 Navier–Stokes solutions for parallel flow in rivulets on an inclined plane. *J. Fluid Mech.* **507**, 367–379.

Pollack, M. G., Fair, R. B. & Shenderov, A. D. 2000 Electrowetting-based actuation of liquid droplets for microfluidic applications. *Appl. Phys. Lett.* **77**, 1725.

Pratap, V., Moumen, N. & Subramanian, R. S. 2008 Thermocapillary motion of a liquid drop on a horizontal solid surface. *Langmuir* **24** (9), 5185–5193.

Press, W. H., Teukolsky, S. A., Vetterling, W. T. & Flannery, B. P. 1992 *Numerical Recipes in Fortran 77*. Cambridge University Press.

Sammarco, T. S. & Burns, M. A. 1999 Thermocapillary pumping of discrete drops in microfabricated analysis devices. *AIChE J.* **45** (2), 350–366.

Schwartz, L. W. 1998 Hysteretic effects in droplet motions on heterogenous substrates: direct numerical simulations. *Langmuir* **14**, 3440.

Schwartz, L. W. 2001 On the asymptotic analysis of surface-stress-driven thin-layer flow. *J. Engng Math.* **39**, 171.

Schwartz, L. W. & Eley, R. R. 1998 Simulation of droplet motion of low-energy and heterogenous surfaces. *J. Colloid Interface Sci.* **202**, 173.

Schwartz, L. W., Roux, D. & Cooper-White, J. J. 2005 On the shapes of droplets that are sliding on a vertical wall. *Physica* D **209**, 236–244.

Smith, M. K. 1995 Thermocapillary migration of a two-dimensional liquid droplet on a solid surface. *J. Fluid Mech. Digit. Arch.* **294**, 209–230.

Stone, H. A., Stroock, A. D. & Ajdari, A. 2004 Engineering flows in small devices: microfluidics toward lab-on-a-chip. *Annu. Rev. Fluid Mech.* **36**, 381.

Subramanian, R. S. & Balasubramanian, R. 2001 *The Motion of Bubbles and Drops in Reduced Gravity*. Cambridge University Press.

Sur, J., Bertozzi, A. L. & Behringer, R. P. 2003 Reverse undercompressive shock structures in driven thin film flow. *Phys. Rev. Lett.* **90**, 126105.

Sur, J., Witelski, T. P. & Behringer, R. P. 2004 Steady-profile fingering flows in Marangoni driven thin films. *Phys. Rev. Lett.* **93** (24), 247803.

Teletzke, G. F., Davis, H. T. & Scriven, L. E. 1987 How liquids spread on solids. *Chem. Eng. Comm.* **55**, 41–82.

Valentino, J. P., Darhuber, A. A., Troian, S. M. & Wagner, S. 2003 Thermocapillary actuation of liquids using patterned microheater arrays. *Mater. Res. Soc. Symp. Proc.* **773**, N10.3.1–N10.3.5.

Zhornitskaya, L. & Bertozzi, A. L. 2000 Positivity preserving numerical schemes for lubrication-type equations. *SIAM J. Numer. Anal.* **37**, 523.